

# Automatic Extraction of Femur Contours from Hip X-ray Images <sup>\*</sup>

Ying Chen<sup>1</sup>, Xianhe Ee<sup>1</sup>, Wee Kheng Leow<sup>1</sup>, and Tet Sen Howe<sup>2</sup>

<sup>1</sup> Dept. of Computer Science, National University of Singapore,  
3 Science Drive 2, Singapore 117543

chenying, eexianhe, leowwk@comp.nus.edu.sg

<sup>2</sup> Dept. of Orthopaedics, Singapore General Hospital,  
Outram Road, Singapore 169608  
tshowe@sgh.com.sg

**Abstract.** Extraction of bone contours from x-ray images is an important first step in computer analysis of medical images. It is more complex than the segmentation of CT and MR images because the regions delineated by bone contours are highly nonuniform in intensity and texture. Classical segmentation algorithms based on homogeneity criteria are not applicable. This paper presents a model-based approach for automatically extracting femur contours from hip x-ray images. The method works by first detecting prominent features, followed by registration of the model to the x-ray image according to these features. Then the model is refined using active contour algorithm to get the accurate result. Experiments show that this method can extract the contours of femurs with regular shapes, despite variations in size, shape and orientation.

## 1 Introduction

Extraction of bone contours from x-ray images is an important first step in computer analysis of medical images. For example, to detect fractures in femur bones from x-ray images [1–3], it is necessary to first determine the contours of the femurs within which features are to be extracted for fracture detection. In the work of [4], contours of carpal bones are determined followed by extracting features within the bone region for skeletal age assessment. Interestingly, most of the existing work on medical image segmentation has been focused on CT and MR images. Much less work has been done on the segmentation of x-ray images.

Classical image segmentation algorithms assume that the regions to be segmented contain homogeneous features. With this assumption, the segmentation algorithms attempt to segment the input image into regions based on feature homogeneity criteria. Unfortunately, such homogeneity criteria are not satisfied for large and complex bones in x-ray images. For instance, in a femur x-ray image (Fig. 1), the femoral head region contains nonuniform texture pattern due to the trabeculae (Fig. 1b), and the femoral shaft region has nonuniform intensity due

---

<sup>\*</sup> This research is supported by NMRC/0482/2000.

to the hollow interior within solid bony walls (Fig. 1a). Moreover, the femoral head overlaps with the pelvis bone. In this case, the extraction of bone contours becomes a more complex problem than classical image segmentation problem. This paper describes a model-based approach for automatically extracting femur contours from standard hip x-ray images used in clinical practice (Fig. 1a).

## 2 Related Work

As discussed in Section 1, classical image segmentation algorithms that rely on region homogeneity criteria are not applicable for the extraction of femur contours in x-ray images. These algorithms include thresholding, region growing, region splitting and merging, watershed, classifier, clustering, etc. [5, 6].

Deformable models such as active contour [7], active shape [8], and level set method [9] have also been used for medical image segmentation [6]. These methods are contour-based instead of region-based. So, they have the potential of extracting contours of body parts that do not contain homogeneous features. An important weakness of these approaches is that they typically require good initialization of the model contour. If the model is poorly initialized, these approaches can be easily affected by noise and extraneous edges in the image, resulting in incorrect segmentation of the regions.

The atlas-based approach [6] can overcome the weakness of deformable models by roughly aligning a spatial map called atlas to the image before applying deformable model methods. That is, it attempts to solve the initialization problem of deformable models by using prior knowledge such as spatial relationships between the body parts in the images. This approach is very promising but it is typically application specific. That is, segmentation of different images of different body parts typically require different kinds of atlas that contain different prior knowledge. This approach has been applied to the segmentation of brain MR images [10, 11] and abdominal CT images [12].

In our application, the atlas-based approach can still face difficulties because the femurs in different images can be oriented differently (Fig. 4) due to variations in the patients' standing postures resulting from femur fractures. Incorporating articulation of body parts in the atlas-based approach may help to solve the problem of model initialization but it makes the atlas very complex and difficult to use. Instead, we apply a simpler model-based approach specific to the femur bone that can handle variations in shape, size, as well as the orientation of the femur in different images.

## 3 Overview of Algorithm

Our algorithm takes a standard hip x-ray image (Fig. 1a) as the input and automatically extracts femur contours in the x-ray image. It is a model-based algorithm that consists of three main stages:

1. Delineation of the regions that contain the left and the right femurs.

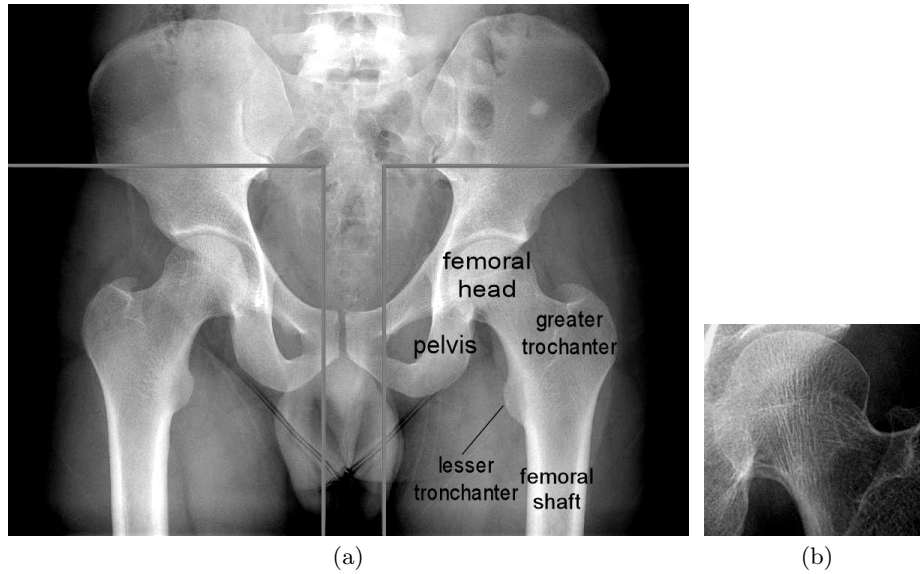


**Fig. 1.** (a) A standard hip x-ray image. The dark lines delineate the regions that contain the femurs. (b) Close-up view of femoral head.

2. Registration of a 2D model femur contour to femur regions in the image.
3. Application of the active contour algorithm with shape constraints to refine the femur model to accurately identify the femur contour in the image.

The first stage is easy to automate because the pose of the patients are similar when the hip x-ray images are taken. The femurs always fall in the left and right bottom corners of the images. Based on 50 training samples, it is determined that the femur region falls within a bounding box of size  $990 \times 1160$  pixels.

The second and third stages are described in the following sections.

### 3.1 Registration of Femur Model

This stage applies prior knowledge about the femur to register a model of the femur contour to the one in the image. It consists of four main steps:

1. Detection of candidate femoral shafts represented by pairs of parallel lines.
2. Detection of candidate femoral heads represented by circles.
3. Detection of candidate turning points near the base of the greater trochanter.
4. Piecewise registration of model femur contour.

#### 1. Detection of Candidate Femoral Shafts

The outer contours of the femoral shaft consists of two approximately parallel straight lines. So, the natural way to detect femoral shaft is to find a pair of long parallel straight lines.

Femoral shaft detection is performed as follows. First, up to 8 points near the bottom of the image with the largest horizontal intensity gradient components are identified. These are good candidate feature points because the points of the shaft contours have very large intensity gradients. The directions of the intensity gradients at these points should not be larger than  $30^\circ$  (determined from training samples) because the shafts are roughly vertical in the images.

Next, contour following method is applied to identify approximately straight lines starting at the points detected above. The points along a line should have roughly the same intensity gradient direction, and fit well onto a straight line.

After identifying all candidate lines, they are paired up to form candidate femoral shaft contours. The lines are paired based on the following criteria:

- The width  $w_i$  between a pair  $i$  of lines should fall within an acceptable range. From training samples, it is found the width has a unimodal distribution which can be modeled by a Gaussian  $G_s$  with a mean  $\mu_s$  of 44.64 pixels and a standard deviation  $\sigma_s$  of 4.67. So, given the width  $w_i$ , the probability that the pair of lines is the shaft contour is given by  $G_s(w_i|\mu_s, \sigma_s)$ .
- The lines in a pair  $i$  have the correct intensity gradient directions. Specifically, the intensity gradient of the line on the left of the femur should change from dark to bright along the positive  $x$ -axis, and that of the line of the right of the femur should change in the opposite direction. Moreover, they should also have large intensity gradient magnitudes  $M_i$ , which is computed as the mean of the intensity gradient magnitudes of the points along the lines.
- Thus, the probability  $P_i$  that a pair  $i$  of lines is indeed the shaft contour is proportional to the product  $M_i G_s(w_i|\mu_s, \sigma_s)$ , assuming the intensity gradient magnitude and the shaft width are independent factors. The intensity gradient magnitude is based on x-ray absorption, while the shaft width is based on the patient’s body size. These two factors are thus independent.

So, each candidate femoral shaft  $i$  is associated with a probability measure  $P_i$ . The top candidates, at most three, with the largest probability measures are kept. Figure 2(a) illustrates an example with two candidate femoral shaft contours.

## 2. Detection of Candidate Femoral Heads

The femoral head is approximately circular. Usually, the contour of the femoral head is not very distinctive. On the other hand, the femur socket of the hip bone appears as strong edges in x-ray images, and the points on these strong edges have very large horizontal or vertical intensity gradient components. So, such points are detected at the top left corner of the femur region in the image. Next, circles are fitted over these points using circular Hough transform.

For a particular patient, the size of the femoral head is positively related to that of the femoral shaft. From training samples, it is found that the ratio of the radius of the femoral head to the width of the femoral shaft has a unimodal distribution which can be modeled by a Gaussian  $G_h$  with a mean  $\mu_h$  of 0.91 and a standard deviation  $\sigma_h$  of 0.11. Given a fitted circle  $i$  with radius  $r_i$  and a

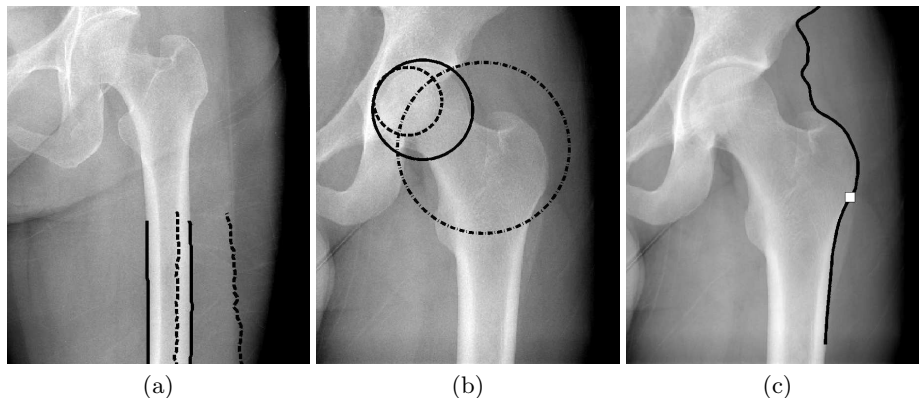


**Fig. 2.** (a) Candidate femoral shafts. (b) Candidate femoral heads. (c) Turning point (white dot) at greater trochanter.

candidate shaft with width  $w_i$ , the probability that circle  $i$  falls onto the femoral head is given by  $G_h(r_i/w_i|\mu_h, \sigma_h)$ . For each candidate shaft found in the previous step, the top femoral head candidates, at most three, with the largest probabilities are kept. This produces at most nine shaft-head combinations. Fig. 2(b) illustrates an example with 3 candidate femoral heads.

### 3. Detection of Candidate Turning Points

In addition to the candidate femoral shafts and heads, an important feature point which we call the “turning point” is also extracted (Fig. 2c). This feature point is required to correctly initialize the model feature contour for running the active contour algorithm. It is obtained as follows:

- For each candidate femoral shaft, the line on the right side of the parallel pair is extended upward using contour following method with the straight line condition relaxed. So, the line now traces a curve that goes along the boundary of the greater trochanter.
- Next the second derivatives of the points along the curve is computed. The locations of the zero crossings of the second derivatives are identified.
- For each shaft-head combination, the candidate turning points along the shaft and below the center of the head are identified.
- The lowest candidate turning points, at most three, are kept for each shaft-head combination. This produces at most 27 shaft-head-turning point combinations.

### 4. Piecewise Registration of Femur Model

The model femur contour is divided by five feature points into five segments (Fig. 3a). The corresponding features points in the image are obtained as follows.

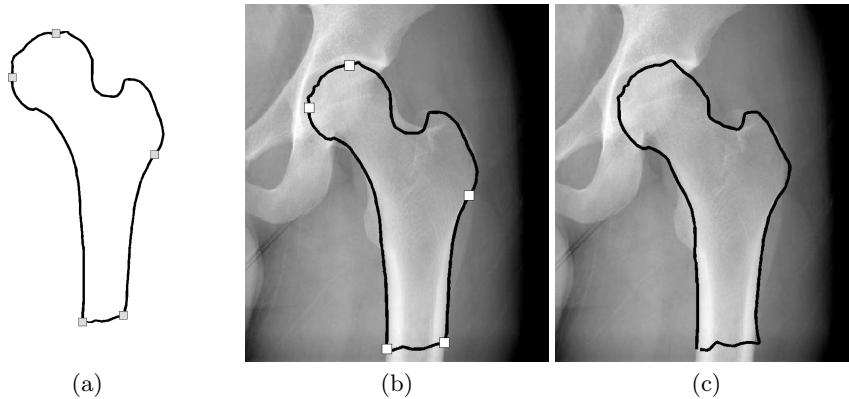


**Fig. 3.** (a) Model femur contour divided into 5 segments. (b) Piecewise registered femur model used as the initial configuration of the snake algorithm. (c) Extracted femur contour after running the snake algorithm.

The two feature points on the head contour are obtained from the top-most and left-most points of a candidate femoral head. The two feature points at the bottom of the shaft contour are obtained from a candidate femoral shaft. The last feature point is a candidate turning point.

The model femur contour is placed onto the image by piecewise registration of the segments based on each of the 27 possible shaft-head-turning point combinations. The registration of each segment is performed by computing the scaling factor  $s$ , rotation matrix  $\mathbf{R}$  and translation vector  $\mathbf{T}$  that maps a model feature point  $\mathbf{p}$  to the corresponding image feature point  $\mathbf{q}$ :

$$\mathbf{q} = s\mathbf{R}\mathbf{p} + \mathbf{T}. \quad (1)$$

All other points along the model contour are mapped in the same way onto the image. Figure 3(a) illustrates a model femur contour that is registered onto the image and to be used as the initial configuration of the active contour algorithm.

### 3.2 Active Contour with Curvature Constraints

The original active contour [7], or snake, algorithm is too flexible for this application and has a high tendency of being attracted to noise and extraneous edges instead of the desired femur contour. To allow the snake to avoid noise and extraneous edges, shape constraints are added to the snake model.

The snake is represented by a parametric contour  $\mathbf{v}(s) = (x(s), y(s))$ ,  $0 \leq s \leq 1$ . Its internal energy  $E_i(\mathbf{v}(s))$  is defined as

$$E_i(\mathbf{v}(s)) = \frac{1}{2} (\alpha \|\mathbf{v}'(s)\|^2 + \beta \|\mathbf{v}''(s)\|^2) \quad (2)$$

where  $\alpha$  and  $\beta$  controls the stretching and bending of the snake contour. It is attracted to image features such as edges and lines. The image features are

represented by the external energy  $E$ . In our application, the gradient vector flow field [13] is used for  $E$ .

The shape of a snake can be constrained by constraining its curvature. The curvature of a contour is proportional to the rate of change of the tangent of the contour, which is a second derivative of the contour point. So, the curvature can be represented by the second derivative vector  $\mathbf{v}''(s) = (x''(s), y''(s))$ .

To constrain the curvature, we introduce a spring force that is proportional to the difference between the actual curvature  $\mathbf{v}''(s)$  of the snake and the reference curvature  $\boldsymbol{\omega}(s)$  of the model. The reference curvature is obtained by averaging the curvature of corresponding points in training samples. Then, the spring energy  $E_c(\mathbf{v}(s))$  is given by

$$E_c(\mathbf{v}(s)) = \frac{\xi}{2} \|\mathbf{v}''(s) - \boldsymbol{\omega}(s)\|^2 \quad (3)$$

where  $\xi$  is a constant parameter that controls the stiffness of the snake. The larger the  $\xi$ , the more stiff is the snake, and thus, the better is the snake in preserving its reference shape encoded by the reference curvature  $\boldsymbol{\omega}(s)$ .

The snake's total energy  $E_T$  is

$$E_T = \int [E_i(\mathbf{v}(s)) + E_c(\mathbf{v}(s)) + E(\mathbf{v}(s))] ds. \quad (4)$$

When  $E_T$  is minimized,  $\mathbf{v}(s)$  satisfies the following Euler-Lagrange equation, which can be obtained using variational calculus:

$$-(\alpha \mathbf{v}'(s))' + (\beta \mathbf{v}''(s))'' + (\xi \mathbf{v}''(s) - \xi \boldsymbol{\omega}(s))'' + \nabla E(\mathbf{v}(s)) = 0. \quad (5)$$

Denote the vectors  $\nabla E = \mathbf{F} = (F_x, F_y)$  and  $\boldsymbol{\omega} = (\omega_x, \omega_y)$ . Discretizing Eq. 5 and rewriting in matrix form yields

$$\begin{aligned} \mathbf{A}_x \mathbf{x} + \mathbf{F}_x &= 0 \\ \mathbf{A}_y \mathbf{y} + \mathbf{F}_y &= 0. \end{aligned} \quad (6)$$

Let the snake be a closed contour with  $n$  points such that  $\mathbf{v}(n+1) = \mathbf{v}(1)$ . Then, the matrix  $\mathbf{A}_x$  is given by

$$\mathbf{A}_x = \begin{bmatrix} c_1 & d_1 & e_1 & 0 & \cdots & 0 & a_1 & b_1 & f_1 \\ b_2 & c_2 & d_2 & e_2 & 0 & \cdots & 0 & a_2 & f_2 \\ \vdots & \vdots \\ d_n & e_n & 0 & \cdots & 0 & a_n & b_n & c_n & f_n \\ 0 & 0 & 0 & 0 & \cdots & 0 & 0 & 0 & 1 \end{bmatrix} \quad (7)$$

where

$$\begin{aligned} a_i &= e_i = \beta + \xi \\ b_i &= d_i = -\alpha - 4\beta - 4\xi \\ c_i &= 2\alpha + 6\beta + 6\xi \\ f_i &= \xi(-\omega_{x,i-1} + 2\omega_{x,i} - \omega_{x,i+1}). \end{aligned} \quad (8)$$

Compared to the original snake,  $\mathbf{A}_x$  has an additional column of constants  $f_i$  that capture the second derivatives of the reference curvature at points  $\mathbf{v}(i)$ .

Moreover, an extra row of  $n$  zeros followed by a 1 is added to make the matrix square and invertible. The matrix  $\mathbf{A}_y$  is the same as  $\mathbf{A}_x$  except  $\omega_x$  in  $f_i$  is replaced by  $\omega_y$ .

Equation 6 can be solved iteratively by regarding  $\mathbf{x}$  and  $\mathbf{y}$  as functions of time  $t$ , yielding the iterative update equations:

$$\begin{aligned}\mathbf{x}(t) &= (\mathbf{A}_x + \gamma\mathbf{I})^{-1}(\gamma\mathbf{x}(t-1) - \mathbf{F}_x(t-1)) \\ \mathbf{y}(t) &= (\mathbf{A}_y + \gamma\mathbf{I})^{-1}(\gamma\mathbf{y}(t-1) - \mathbf{F}_y(t-1)).\end{aligned}\tag{9}$$

The constrained snake algorithm is applied onto each of the candidate shaft-head-turning point combinations. After the snake algorithm has converged, the shape difference between the candidate resultant snake and the reference model is computed in terms of the mean squared error of rigid registration between them. The candidate result with the smallest shape difference is regarded as the extracted femur contour.

Existing methods that also incorporate geometric constraints in the snake include [11, 14]. Shen et al. [11] embedded geometric information as attribute vector into a snake. The attribute vector contains the areas of triangles formed by each point on the snake and their two neighboring points. During the snake’s evolution process, the areas of the triangles are constrained. However, triangles of different shapes can have the same area. So, this method may not reliably constrain the snake’s shape.

Foulonneau et al. [14] includes Legendre moments in the snake. The shortcoming of this method is that moments provide global description of a reference shape. Large local deformations such as size variations of parts of the femur and orientation variations of femurs in different images (Fig. 4) would change the moments significantly even though the overall shape remains roughly the same. Moreover, this method will become very complex if rotation invariance, left out in [14], is to be considered as well.

In comparison, our method not only allows the snake to handle shape and size variations but also variations in the orientations of the femurs.

## 4 Tests and Discussion

A training set of 100 femur images with manually extracted contours were used to determine the shaft width model and the femoral head radius model. A different set of 172 femur images were used to test the contour extraction method. The size of all training and testing images was  $297 \times 348$ . A simple model femur is used by the algorithm to extract the femur contours in the test images. The error of an extracted contour is measured in terms of the mean error between the points on the extracted contour and their corresponding points on the manually marked contour. Success rate is the fraction of testing samples whose femur contours are extracted accurately. A femur contour is considered successfully extracted if the error is less than 8 pixels, which is only 2% of the image size.

Of the 172 testing samples, 81.4% of the femur contours were successfully extracted, despite the variations in shapes, sizes and orientations of the femurs

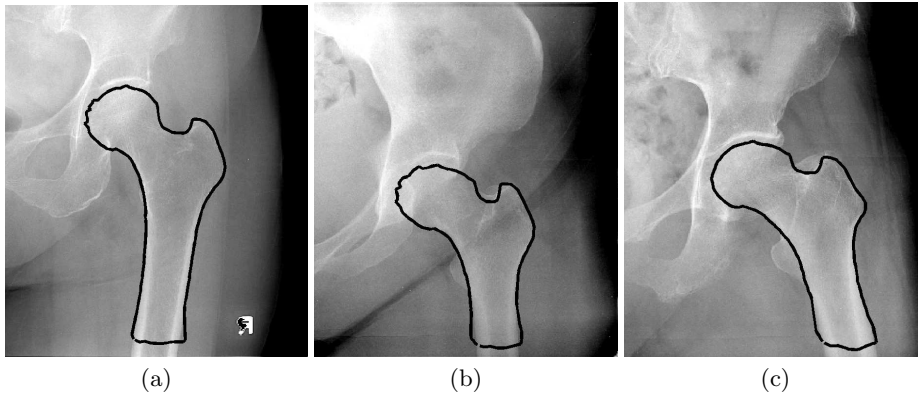


**Fig. 4.** Sample test results. Despite the significant variations in the shapes, sizes, and orientations of the femurs in the images, correct femur contours are extracted. The errors are: (a) 0.98 pixel (b) 3.27 pixels (c) 3.92 pixels

in the images (Fig. 4). The mean and standard deviation of the errors of the successful samples are 3.88 pixels and 1.50 pixels.

Among the failed cases, 31.3% are such that at least one of the candidate solution is acceptable but not the top ranking solution (e.g., Figure 5a). If we consider these cases as successful cases, the success rate becomes 87.2%.

The other 68.7% of the failed cases do not have acceptable results among the candidate results. Failed samples are either fracture cases such as Figure 5(b) or healthy femurs with odd shapes such as Figure 5(c) or images that contain artifacts such as extraneous straight lines caused by the analogue imaging process. Odd shaped femurs have very short neck or shaft or both, due to the unusual standing postures of the patients with fractures on the other femurs.

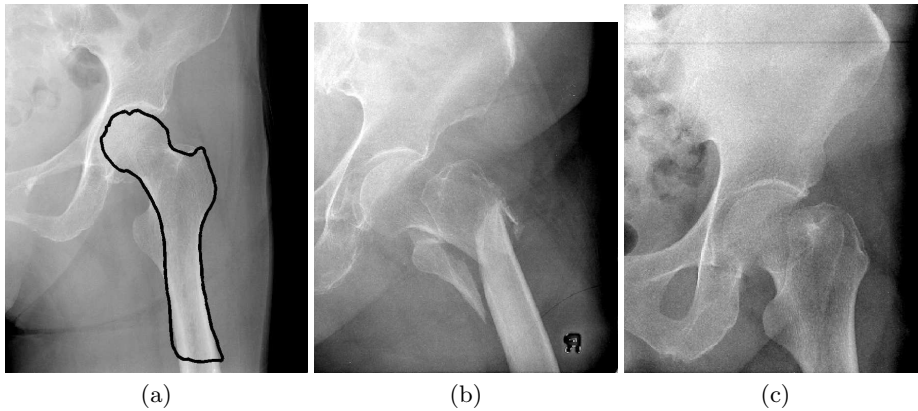


**Fig. 5.** Sample failed cases. (a) One of the candidate solution is acceptable but not ranked at the top. (b) Fractured femur with severe shape distortion. (c) Healthy femur with an odd shape. There is almost no neck or shaft.

## 5 Conclusion

This paper presented a method for automatically extracting femur contours from x-ray images. The method detects the positions of the femoral shaft, head and turning points. Then, a model femur contour is registered piecewise to the x-ray image according to these detected features. Finally, active contour with shape constraints is applied to accurately identify the femur contour. Experiments show that this method can successfully extract the contours of femurs with regular shapes, despite variations in size, shape, and orientation. Our continuing research is to extend the method to the extraction of the contours of femurs with severe shape distortions and of other body parts in x-ray images.

## References

1. Chen, Y., Yap, W.H., Leow, W.K., Howe, T.S., Png, M.A.: Detecting femur fractures by texture analysis of trabeculae. In: Proc. ICPR. (2004)
2. Lim, S.E., Xing, Y., Chen, Y., Leow, W.K., Howe, T.S., Png, M.A.: Detection of femur and radius fractures in x-ray images. In: Proc. 2nd Int. Conf. on Advances in Medical Signal and Information Processing. (2004)
3. Lum, V.L.F., Leow, W.K., Chen, Y., Howe, T.S., Png, M.A.: Combining classifiers for bone fracture detection in x-ray images. In: Proc. ICIP. (2005)
4. Lin, P., Zhang, F., Yang, Y., Zheng, C.: Carpal-bone feature extraction analysis in skeletal age assessment based on deformable model. *J. of Computer Science and Technology* (2004)
5. Rogowska, J.: Overview and fundamentals of medical image segmentation. In Bankman, I.N., ed.: *Handbook of Medical Imaging, Processing and Analysis*. Academic Press (2000) 69–85
6. Pham, D.L., Xu, C., Prince, J.L.: Current methods in medical image segmentation. *Annual Review of Biomedical Engineering* **2** (2000) 315–337
7. Kass, M., Witkin, A., Terzopoulos, D.: Snakes: active contour models. *Int. J. of Computer Vision* **1** (1987) 321–331
8. Cootes, T.F., Hill, A., Taylor, C.J., Haslam, J.: The use of active shape models for locating structures in medical images. *Image and Vision Computing* **12** (1994) 355–366
9. Sethian, J.A.: *Level Set Methods*. Cambridge University Press (1996)
10. Aboutanos, G.B., Nikanne, J., Watkins, N., Dawant, B.M.: Model creation and deformation for the automatic segmentation of the brain in MR images. *IEEE Trans. on Biomedical Engineering* **46** (1999) 1346–1356
11. Shen, D., Herskovits, E.H., Davatzikos, C.: An adaptive-focus statistical shape model for segmentation and shape modeling of 3-D brain structures. *IEEE Trans. on Medical Imaging* **20** (2001)
12. Park, H., Bland, P.H., Meyer, C.R.: Construction of an abdominal probabilistic atlas and its application in segmentation. *IEEE Trans. on Medical Imaging* **22** (2003) 483–492
13. Xu, C., Prince, J.L.: Gradient vector flow: A new external force for snakes. In: Proc. IEEE Conf. on CVPR. (1997)
14. Foulonneau, A., Charbonnier, P., Heitz, F.: Geometric shape priors for region-based active contours. In: Proc. ICIP. (2003)